JOURNAL OF SPACECRAFT AND ROCKETS
Vol. 30, No. 4, July–August 1993

Window Cooling Technology Program

R. A. Hodge* and P. Raghuraman†
Aerojet Propulsion Division, Sacramento, California 95813
and
A. L. Murray‡
Aerotherm Corporation, Huntsville, Alabama 35806

A development effort is underway on the window cooling technology (WCT) program to design an actively cooled mosaic window system for use on hypersonic interceptors with infrared seekers. The cooling system provides window temperature control through film cooling using supersonic gas or liquid droplet coolants ejected over the surface of each window. Coolants are distributed through the conical array of windows by a lattice platelet frame. A novel liquid-ejection approach has been assessed via a droplet diameter test series. Potential window element optical issues have been identified and eliminated with parametric optical analysis and testing. Thermal issues were extensively explored through arcjet testing at the NASA Ames 60-MW facility. This arcjet series resulted in a chemically reactive coolant, NO_2/N_2O_4, which has a thermal performance significantly higher than the predicted inert values. Computational fluid dynamics (CFD) analysis of both arcjet and flight cases have successfully modeled this reactive coolant, resulting in additional insight into its behavior.

Nomenclature

C_p =specific heat
C_h =local heat transfer coefficient
M =Mach number
q =heat flux
S =coolant ejection slot height
T =temperature
T_{ad} =adiabatic temperature
T_t =total temperature
T_{ta} =total arcjet temperature
U =velocity
χ =location along window length
η =coolant efficiency
μ =viscosity
ρ =density
ξ =film cooling correlation parameter

Subscripts

c =coolant condition
e =external boundary-layer edge condition
u =measured uncooled calibration test quantity
w =measured cooled test wall quantity

Introduction

THE objective of the window cooling technology (WCT) program is to develop the window cooling technology necessary to enable hypersonic interceptor sensor performance in this stressing thermal and signal-distorting environment. Previous interceptors have been limited in intercept range due to an upper bound on the speed these interceptors have been able to achieve without window cooling. Without window cooling, window temperatures rise to such a level that the target signal is lost to background infrared (IR) window emission or distorted due to aero-optic noise. Aero-optic noise is chiefly due to a blurring of the incoming light by density fluctuations in the mixing layer between the window coolant and the hot airflow. The index of refraction of a gas is dependent on its density.

These aero-optical errors can be reduced by a mosaic cooling system (Fig. 1). A mosaic pattern of windows is employed instead of one window to increase thermal efficiency and to reduce the thickness of the mixing layer as illustrated in Fig. 2. Reducing the mixing-layer thickness decreases aero-optic noise as blur due to density fluctuations is path length dependent.

The mosaic concept is essentially a cone consisting of a number of windows held together by a metallic frame structure made of platelets. These platelets are thin sheets of metal which have been individually chemically etched with coolant passageways and coolant-ejection control features. The individual platelets are then stacked together and placed under a load in a diffusion bonding furnace to yield a monolithic part. The platelet frame creates the coolant management system between the small windows. The size of any leg of this frame remains small enough that the frame itself is merely a screen about the windows. This has led the concept of a mosaic cone to be called a transparent cone or a transparent forebody.

The vehicle advantage of a transparent forebody is that the seeker aperture can be reasonably close to the diameter of the base

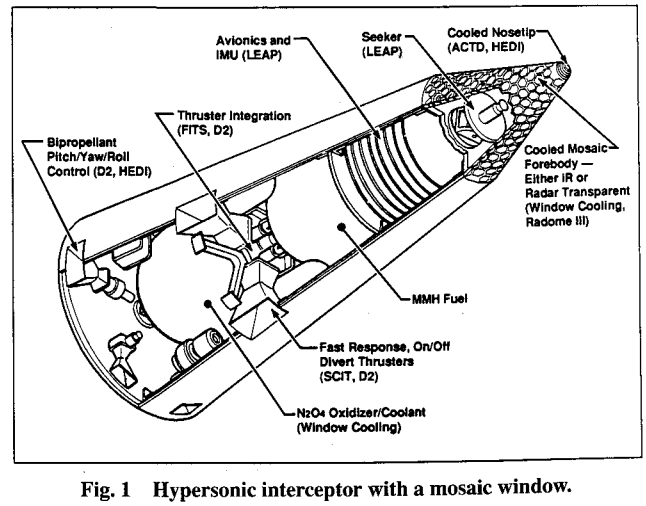

Fig. 1 Hypersonic interceptor with a mosaic window.

Presented as Paper 92-2803 at the AIAA/SDIO Annual Interceptor Technology Conference, Huntsville, AL, May 19–21, 1992; received Aug. 17, 1992; revision received Dec. 14, 1992; accepted for publication Dec. 14, 1992.

*Project/Design Engineer, Building 2019, P.O. Box 13222. Member AIAA.
†Senior Engineering Specialist, Building 2019, P.O. Box 13222. Member AIAA.
‡Principal Engineer, 1500 Parameter Parkway, Suite 225. Senior Member AIAA.

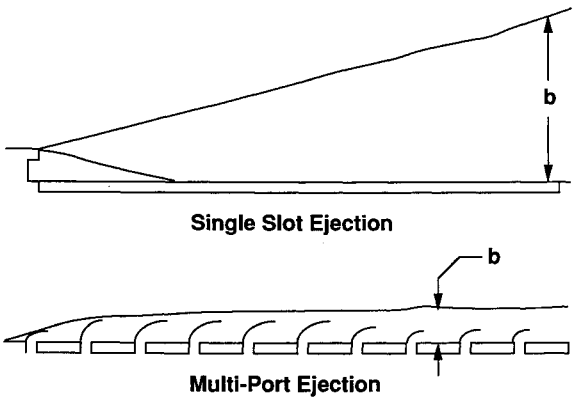

Fig. 2 Single slot and mosaic mixing thicknesses.

of the forebody. Previous single-window designs have had configurations where the size of the seeker has been limited to a small fraction of the vehicle diameter. Aperture area should be maximized to increase acquisition range and resolution whereas vehicle diameter must be minimized to decrease vehicle weight and cost.

In addition to the development of a mosaic window cooling system, a novel method of film cooling has evolved on the WCT program through both testing and analysis. Classical film-cooling approaches have relied on an inert coolant to provide a blanket of coverage over the surface being cooled as the hot airstream mixes with the coolant. The only real variation on this theme has been the heat of vaporization of the coolant. It has been demonstrated on the WCT program that reactive coolants, such as NO_2 and N_2O_4, can greatly increase film cooling efficiencies over inert levels. These coolants dissociate endothermically when heated in the mixing layer, thus absorbing energy. The energy absorbed by these reactions allow NO_2 to perform 5 to 7 times better, by mass flow rate, than its expected inert efficiency.[1]

NO_2 and N_2O_4 have additional system advantages. N_2O_4 is commonly carried onboard hypersonic interceptors as a maneuvering thruster oxidizer. By using N_2O_4 as a window coolant, it is no longer necessary to have onboard a large-volume gaseous coolant tank. N_2O_4, stored as a liquid and more thermally effective, occupies 1/27 the volume of gaseous N_2. Helium requires even more storage volume. In previous designs, gaseous coolant tanks have effectively sized the interceptor vehicle.

N_2O_4 can be ejected directly into the boundary layer in the form of a liquid or can be gasified into NO_2 via a heat exchanger or gas generator prior to ejection. Both of these methods are being explored.

Liquid-ejection film cooling, a new approach for window cooling, was initially a high-risk approach as the droplets ejected by this method cannot be allowed to significantly effect the optical signal. A WCT droplet-sizing test provided data that has reduced this risk.

Windows formed around the surface of a cone can follow the contour of the cone, which may lead to a blurring prescription in the windows, or can be made flat which may cause aerodynamic perturbations in the flowfield. An uncooled optical test series and its supporting analysis were used to investigate this problem and have resulted in a design approach that minimizes both of these effects.

A thermal test series conducted in the 60-MW arcjet at NASA Ames has yielded data on the reactive coolant NO_2 and has provided data on different ejection techniques, coolant carryover effects, and window length effects for mosaic window concepts.

Extensive CFD analysis has been conducted on this arcjet test series, on liquid ejection of N_2O_4, and on flight configurations.

Liquid-Ejection Splashplate Elements

Early on in the program, it was identified that a coolant ejected as a liquid instead of a gas would result in a reduction of the optical blockage associated with the mosaic manifolding system. Additionally, for the case of N_2O_4 as a window coolant, liquid ejection would eliminate the need for a heat exchanger for N_2O_4 gasification and would allow colder window temperatures. The difficulty of using a liquid-ejection technique is the possible optical problems (such as light scattering) due to droplets in the boundary layer.[2]

Predictions were made on the intensity ratio of a signal passing through a cloud of micro-droplets. These results are shown in graphs of intensity ratio vs droplet radius to wavelength ratio for different cloud thicknesses at various wavelengths. Figure 3 plots this ratio for the case of a 3.5-μm signal.

The splashplate window coolant-ejection element is modified from a platelet rocket-injection element which has been developed over the last twenty years specifically to create small droplets of rocket fuel which mix more rapidly and thus increase combustion efficiency. Pressure in the ejection element is kept high until just prior to release into the boundary layer. This configuration allows the N_2O_4 to be rapidly brought from a temperature and pressure at which it is a liquid to a condition of the same temperature, but lower pressure, where the substance is theoretically a gas. This effect is called "flashing" the substance. Unfortunately, flashing, which is often considered an "instantaneous" process, actually requires a finite amount of time. The flowfield over the surface of a hypersonic vehicle will rapidly accelerate these droplets from the ejection point to the window. To be conservative, it is assumed that the droplets will not flash, and thus minimum droplet size is sought. It should be noted that this strategy will also greatly reduce flashing time.

Two experimental platelet stacks were fabricated, each with a series of different splashplate liquid-ejection elements. These elements differed from each other in their design parameters such that a parametric study could be made on the effect of element geometry on droplet size. To measure droplet size, a Malvern laser system at Aerojet was employed. The Malvern laser system uses the scatter from a laser beam passed through a cloud of particulates to measure the size distribution of those particulates.[3] Parametric trades on supply pressure and geometry effects were conducted using water, allowing for greater sensitivity in the results as water forms larger, more easily measured, droplets than N_2O_4. Tests conducted to assess the feasibility of using liquid ejection for a window coolant were conducted with freon serving as a surrogate for N_2O_4. This is common practice for N_2O_4 droplet-sizing experiments due to the virtually identical shear and vaporization properties of N_2O_4 and freon at the tested conditions. Shadowgraph tests were also conducted on this hardware to determine larger effects, such as element and interelement coverage of coolant.

The Malvern system generated plots of the percentage of the total droplets that were of a certain size and supplied additional statistical information as well. From the parametric tests with water, it was determined that the effect of higher pressure drop over the element was small; the droplet size is inversely proportional to roughly the square root of the pressure drop. Droplet diameter is also roughly proportional to the square root of the control orifice diameter for the range of orifices tested, although theory predicts an adverse departure from this for extremely large orifice diameters.[4] The splashplate fan half-angle has an optimum

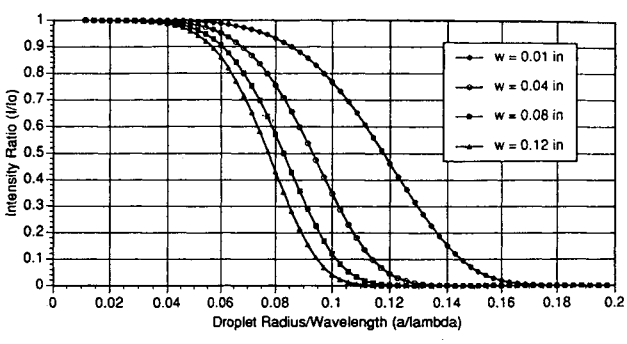

Fig. 3 Intensity ratio vs droplet radius/signal ratio for varying coolant-layer thicknesses (w) at 3.5 μm.

range greater than which flow instabilities occur and under which droplet size increases due to a thickening of the sheet of liquid produced. The large-angle effect has been shown in previous tests whereas the small-angle effect was demonstrated in this test series.

One of the greatest effects on droplet size was the dynamic pressure of nitrogen flowed over the surface of the model to simulate airflow over the part. This flowfield shattering of the droplets by a supersonic flow has been well studied in the hypersonic vehicle area for fuel injection.[5] The difference between that data and this test was the initial size of the droplets before being exposed to the airflow. The droplets in this study were introduced into the flow at much smaller sizes, but the effect on the ratio of the diameter of shattered droplets vs the diameters of unshattered droplets was similar to the larger droplet studies.

Tests conducted with freon as a surrogate for N_2O_4 yielded very promising results. The Malvern equipment is only calibrated to measure droplet sizes of 1.2 μm and above, although the device will measure and record smaller sizes. Only 10% of the droplets measured were over this 1.2-μm diameter. The highly conservative assumption was made that the average droplet size was 1 μm.

The aforementioned case was conducted with nitrogen simulating the external flowfield. This nitrogen, however, was at a small fraction of the dynamic pressure of a typical flight and was at room temperature as opposed to the multithousand-degree temperatures of flight. Figure 4 predicts droplet diameters for N_2O_4 as a function of flight dynamic pressures. As can be seen on this figure, droplet sizes in flight are predicted to be much smaller than one-quarter of a wavelength for the IR wavelengths of interest (3.5–10 μm). This calculation makes the conservative assumption that vaporization does not occur. Flight designs will attempt to flash the liquid into a gas before passing over the window.

Spark shadowgraphs were conducted on both single splashplate elements and on a window's complement of splashplate elements. The single-element shadowgraphs revealed a healthy fan of droplets without extreme bias in droplet concentration spatially as the fan expanded. Shadowgraphs of a row of splashplates such as would be present on the forward edge of a window revealed a continuous coverage of the cooled surface. No appreciable breaks were visible between elements which might result in thermal streaking.

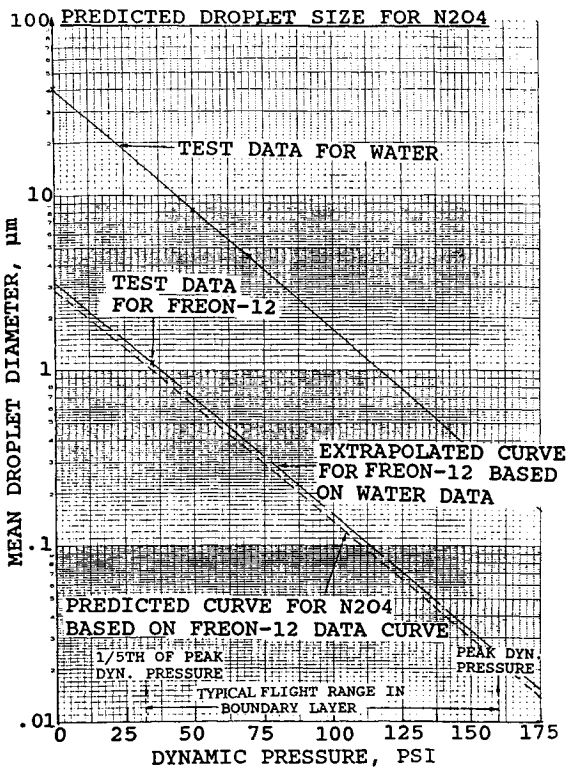

Fig. 4 Droplet sizes for flight without vaporization.

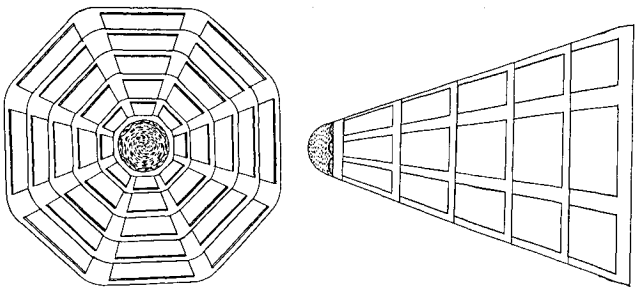

Fig. 5 Octacone configuration.

Both the analysis and the test data obtained from this study have indicated that an IR window cooling system using splashplate liquid ejection is indeed feasible. Future testing on WCT will evaluate the aero-optical effects of liquid ejection.

Window Pane Geometry

The second test series conducted on this program was the uncooled cone test series. When covering the surface of a cone with a number of small windows, these windows can either conform to the curving surface of the cone or can approximate the surface of the cone with flat windows.

Windows that follow the curvature of the conical surface cause a "lensing" effect. Light rays striking the windows are bent by the curvature of the windows, resulting in a blurring of the signal. The difficulty with this lens effect for a conical surface is that the curvature of the cone varies with axial distance down the cone. For a stationary seeker, it is possible to form a prescription in the backside of the windows which will effectively bend the light back into its original orientation. With a gimbaling seeker, however, the problem becomes more complex as the correction required is a function of gimbal angle. To accomplish this, a mechanized lens system must be used which actively corrects the optical signal with seeker rotation. Even with such a complex system in operation, minor misalignments in the installation of the window elements would greatly effect the performance of the window system as the focus of the cone would be other than expected.

Small flat windows locally superimposed on a conical surface do not cause the distortions apparent in curved windows. The flat windows, however, will always cause forward and rearward steps when superimposed on a conical (curved) surface. For a given window width, the size of these steps will increase with smaller cone radii. The aero-optical and aerothermal implications of these steps make this choice not the selected configuration.

A third transparent forebody geometry option is to approximate the conical surface with facets that run down the length of the forebody. These continuous flat surfaces allow for flat windows while remaining "aerodynamically smooth" for a zero angle of attack. Figure 5 shows such a "polycone" configuration, in this case an eight-sided "octacone."

Optical analysis of these different window and forebody configurations was performed by Hughes using Code 5 software.[6] Analysis for flight was made using hexigonal windows, whereas analysis corresponding to the Uncooled Cone Optical Tests was conducted using circular windows. The forebody designs analyzed had a 1-in. diameter metallic nose. Parametric studies were conducted on the effect of platelet, window, and cone geometries on blur, transmission, and acquisition range. The mosaic cone design was adjusted where appropriate.

The blur (due to diffraction effects and waveband) for a cone with flat windows was shown to be acceptable. There is a slight benefit to having the platelet frame thickness be equal to that of the window thickness.

The blur shape for a curved window shown in Fig. 6 reveals astigmatism. This noncircular and nonrandom blur shape would require either optical or software correction. Blur diameter for the curved window design was 6 mrad, which was considered unacceptable.

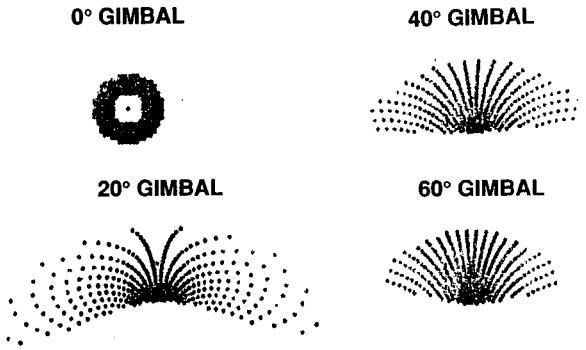

Fig. 6 Curved-window blur shape as a function of gimbal angle.

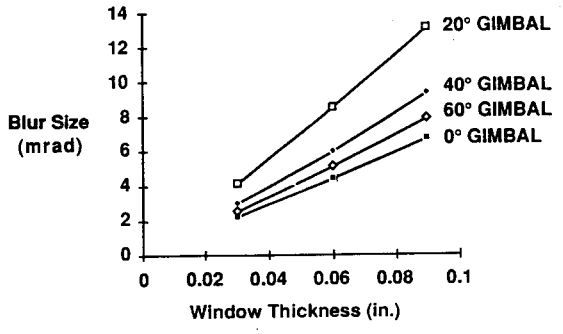

Fig. 7 Curved-window distortion.

Figure 7 shows the effect of window thickness on blur size for a curved window system as a function of seeker gimbal angle. It should be noted that since this lens-effect blur is path length dependent, extremely thin windows would avoid this problem. Such windows are feasible using diamond as a window material with small window sizes. These small window sizes, however, increase optical blockage due to the added platelet frame structure required.

An attempt was then made to correct for lens-effect blur by changing the interior contour of the window surface. The local curvature of the inside window surface was shaped to bend the light back to its original orientation. This resulted in an improvement of about 20% for a fully gimbaling seeker. If the seeker was restricted to gimbal between 20 and 60 deg, an improvement of 50% was achieved.

A system with variable correction on the seeker itself was next explored. Two attempts were made in this area. For the first, a toroid lens, was placed on the seeker. The toroid lens had different optical power in each axis. Since the toroid was fixed relative to the seeker, the seeker must roll to the proper angle when gimbaled in the azimuth direction. This correction approach met with only limited success. The final correction attempt involved two correcting lenses with cylindrical power while maintaining the corrected inner prescription of the curved windows (Fig. 8). One corrector can be rotated as a function of gimbal angle. The cylindrical power of the two lenses adds or cancels depending on the rotation positions selected. The sensor is allowed to refocus for each gimbal angle. This correction technique reduced the blur to acceptable levels of under 1 mrad. The disadvantage of this approach is the fabrication of such a complex optical system.

Other lens-effect corrections that were explored were deformable mirrors, uniquely shaped windows, and a "binary" or holographic surface on the inside of the windows.

Based on this analysis and aero-optical considerations, a polycone design with a larger window spacing of 1.1 in. was chosen as the new WCT baseline approach, given the level of complexity of the mechanized correction system, the higher blockage of the thinner window system, and the aero-optic effects of flat windows superimposed on a conical surface.

To verify this analysis, a test series involving uncooled models was conducted. Three models were designed and fabricated for this test. Figure 9 is a photograph of these cones, all of which have a nominal cone diameter of 5 in. with a cone half-angle of 20 deg. The curved and polycone models were made with plastic window material whereas the cone with superimposed flat windows used quartz windows.

Optical testing of the uncooled cones supported the results of the optical analysis. Both transmission and resolution (which is inversely related to blur) tests were conducted. The resolution of the curved-window model expressed in terms of the modulation transfer function (MTF) as a function of gimbal angle is illustrated in Fig. 10.

Arcjet Thermal Testing

As part of the WCT program, a thermal test series was performed at the NASA Ames 60-MW arcjet comparing the film-cooling effectiveness of a variety of coolants and ejection geometries. The tests involved multiport ejection devices called coupons located on the surface of a 15-deg wedge that was immersed in the arcjet. The coolants used were N_2, CO_2, and NO_2. N_2 was tested to provide a bench mark comparable to previous hypersonic window cooling studies. NO_2 was chosen due to its significant vehicle advantages. CO_2 was tested as an alternate candidate.

The objectives of the WCT test series at NASA Ames were 1) to compare and rank the cooling performance of the candidate coolants, 2) to assess the validity of the superposition principle in determining the downstream cooling benefits of multiple port ejection, 3) to determine the influence of window length on coolant efficiency, and 4) to compare the cooling efficiency of angle ejection with tangential ejection.

The NASA Ames 60-MW arcjet is a facility mainly oriented to low-pressure re-entry vehicle testing. To create a new condition,

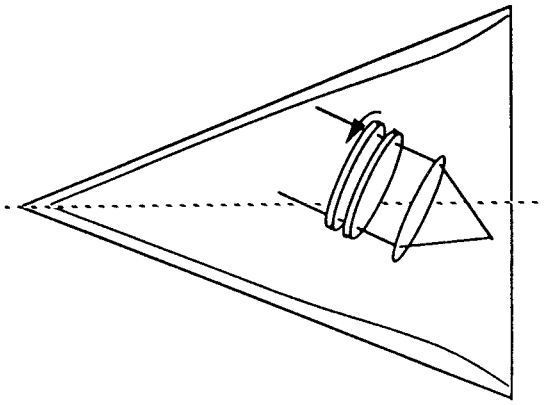

Fig. 8 Corrected curved-window configuration.

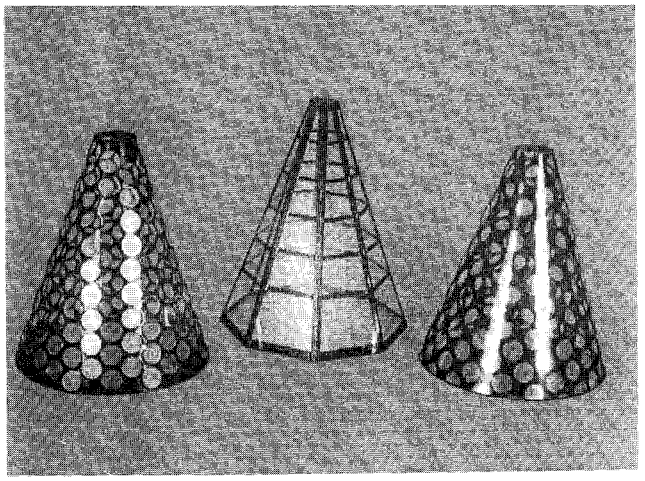

Fig. 9 Uncooled cone optical models.

lower in temperature and higher in pressure, and to fully describe that condition, a series of calibration tests were conducted. These tests consisted of heat flux and pressure sweeps to initially choose the condition and establish flow uniformity, Teflon wedge runs to indicate abnormalities in the flowfield, such as shock impingement, and both heat flux and pressure-instrumented wedges to define the conditions over the test article.

Several different cooled metallic platelet window coupon designs were used, differentiated according to the number of windows present (each window having one row of film-cooling ejection ports) and the type of ejection. The first design consisted of a panel of three windows, each 1.1 in. long and 1 in. wide with coolant ejection located immediately upstream of each window. The second design consisted of a panel of five windows, each 0.6 in. long and 1 in. wide with coolant ejection immediately upstream of each window. Ejection techniques included tangential and angled ejection. Figure 11 illustrates the 1.1-in. angled ejection design.

Coolant ejection occurred through a series of supersonic nozzles with area ratios of about 1.92 (corresponding to Mach 2 for NO_2) laid across the width of the window. The gas coolant was ejected either at a 30-deg angle to the surface or tangential to the surface.

Table 1 shows the matrix of test configurations. During each test run, the coolant flow rates for the front coolant slot and downstream coolant slots would be alternatively stepped down (or up) over several values insuring that each run yielded several sets of thermal data for each combination of coolant flow rates.

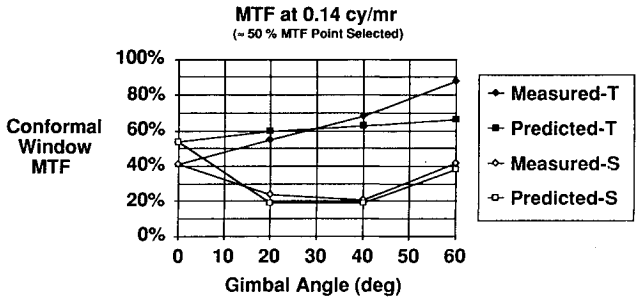

Fig. 10 Comparison of analysis and test data for curved-window resolution.

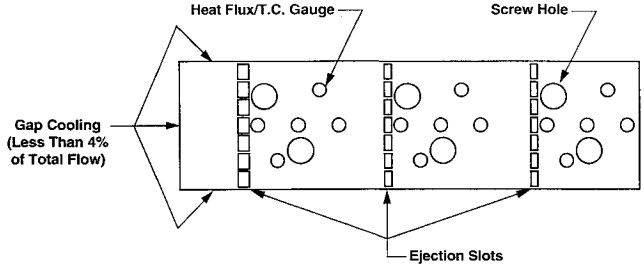

Fig. 11 Typical Ames coupon.

Table 1 Ames arcjet test matrix

Coolant	Ejection type	Enthalpy, Btu/lbm	Slot mass flow range, lbm/s
GN_2	1.1 in. angled	4200	0.007–0.050
	1.1 in. angled	5100	0.005–0.050
	1.1 in. tangent	4200	0.003–0.050
	0.6 in. angled	4200	0.003–0.050
GCO_2	1.1 in. angled	4200	0.003–0.050
GNO_2	1.1 in. angled	4200	0.004–0.013

Table 2 Ames arcjet boundary-layer edge conditions

	Low enthalpy case, 4200 Btu/lbm	High enthalpy case, 5100 Btu/lbm
T_{oe}, °R	8814	9943
T_e, °R	6677	7906
$\rho_e U_e$, lbm/ft^{2}s	7.6	6.1
U_e, ft/s	7323	8143
μ_e, lbm/ft·s	7.2 (10^{-5})	8.2(10^{-5})
M_e	1.8	1.8

Table 3 Fully cooled first window flow rates

Coolant	Flow rate, lbm/s
N_2	0.25
CO_2	0.30
NO_2	0.035

Thermal data for each test run yielded measured surface temperatures and heat fluxes at each thermocouple/heat flux gauge location on the coupon. The primary quantities used for film-cooling analysis are adiabatic wall temperatures. These are deduced from T_w and q_w using the reference heat transfer coefficient method through the relationship

$$T_{\text{ad}} = T_w + q_w / C_h \tag{1}$$

Values for C_h are calculated from the calibration heat flux runs as

$$C_h = q_u / (T_{ta} - T_u) \tag{2}$$

Approach to Thermal Data Reduction and Analysis

To quantitatively compare film-cooling performance of 1) the candidate coolants and 2) angled vs tangential ejection, focus was placed on the front coolant ejection slot which cools the first window section. The primary performance quantities examined were the calculated adiabatic temperatures cast in terms of a coolant efficiency η defined as

$$\eta = (T_{\text{ad}} - T_{te}) / (T_{tc} - T_{te}) \tag{3}$$

As originally established on the HEDI program for N_2 and subsequently modified for more general coolants, η was correlated with the specific heat ratio version of the SAIC correlation parameter ξ defined as follows[7]:

$$\xi = \frac{X}{S^{1.25}} \frac{(\rho U)_e}{(\rho U)_c^{1.25}} \left(\frac{\rho_c}{\rho_e}\right)^{0.4} \frac{\mu_e}{\mu_c^{0.75}} \left[1 + \frac{(\gamma_c - 1)}{2} M_c^2\right]^{0.5} \left(\frac{Cp_c}{Cp_e}\right)^{0.9} \tag{4}$$

The edge values were derived by using the planar ASCC code such that wedge calibration heat fluxes and pressures are matched.[8] Table 2 catalogs edge conditions determined for both low- and high-enthalpy data.

To gauge downstream effects of multiple window designs, including window length, the method of superposition was used.[9] This method uses single, front slot cooled, window coolant efficiency as a building block. The net coolant efficiency over any downstream window due to coolant ejections at several upstream locations is calculated as the superposition of coolant efficiencies of each upstream ejection slot (each flowing by itself).

Thermal Test Results and Data Analysis

To quantitatively compare the relative film cooling performance of candidate gas coolants (N_2, CO_2, and NO_2), front slot (first window) efficiencies for test runs at the 4200 Btu/lbm enthalpy conditions using the 1.1-in. angled ejection coupon are plotted against the film cooling parameter in Fig. 12. A figure of merit typically

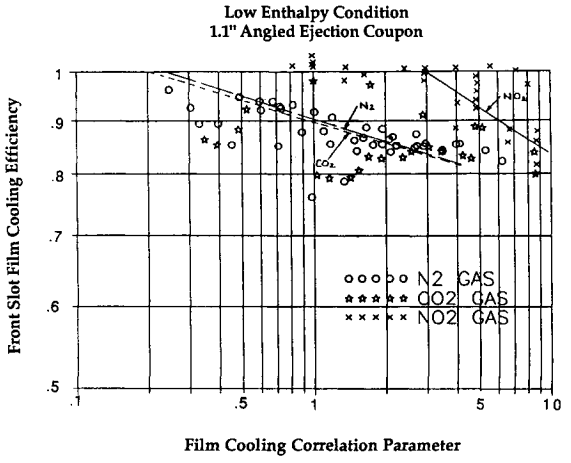

Fig. 12 Relative performance of gas coolants.

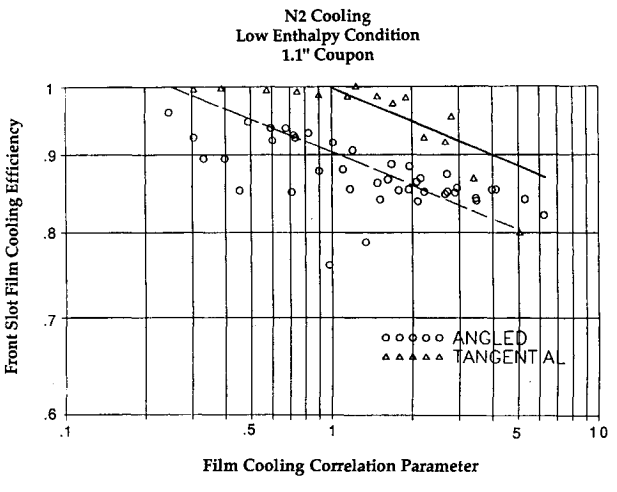

Fig. 13 Angled vs tangential ejection.

used to compare coolants is the "breakpoint," the value of ξ at which the cooling efficiency departs from one. The breakpoints for N_2 and CO_2 are comparable with values of 0.25 and 0.20, respectively. However, the breakpoint for NO_2 is higher by over an order of magnitude with a value of 3.

The higher the value of the breakpoint, the more effective the coolant. Accordingly, NO_2 is the most effective gas coolant followed by N_2 and CO_2 (which are comparable to each other). Based on the specific heat ratio version of the SAIC film-cooling correlation with measured coolant breakpoints, the flow rates required to isothermally cool the 1.1-in. angled ejection front window for the 4200 Btu/s enthalpy NASA Ames condition are shown in Table 3.

It is suggested that the relatively small NO_2 flow requirements are due to the endothermic chemical dissociation of NO_2:

$$2NO_2 \Leftrightarrow 2NO + O_2 \tag{5}$$

For quantitative comparisons of angled and tangential ejection with N_2 as a coolant at 4200 Btu/lbm, front slot film-cooling efficiencies vs ξ are plotted in Fig. 13. The N_2 breakpoint for tangential ejection is 1.0, as opposed to 0.25 for angled ejection. Therefore, tangential ejection is thermally superior to angled ejection film cooling.

To qualitatively gauge the effects of window spacing (or window length) on film-cooling performance, two test runs at the 4200 Btu/lbm enthalpy arcjet conditions using the 1.1-in. window spacing coupon (with 3 windows) and the 0.6-in. window spacing coupon (with 5 windows) were considered. Both used N_2 as a coolant with virtually identical flow rates. The flow rates from the first window slots were 0.05 and 0.048 lbm/s, respectively, whereas the flow rates out of any of the downstream slots of the 1.1-in. window length, 3-window coupons were equal to the sum of the coolant flow rates from any two slots of the 0.6-in. window length, 5-window coupons. The total flow rate to cool the same overall length was, thus, the same.

Figures 14 and 15 compare both heat flux and temperature profiles along the coupon length for the 1.1-in. window length, 3-window design and the 0.6-in. window length, 5-window design. For the same amount of total coolant flow rate and the same total cooled area, the 0.6-in. window length coupon had lower measured peak temperatures and heat fluxes and therefore was more thermally effective.

The superposition principle was applied to an N_2-cooled test run using a 1.1-in. window spacing, 3-window coupon with angled ejection at the 4200 Btu/lbm enthalpy case. The principle used the film-cooling correlation with measured angled ejection front slot breakpoints of 0.25 and efficiency slopes of -0.11 to be the building block for coolant efficiencies. Figure 16 compares measured and calculated coolant efficiencies along the coupon length. This figure demonstrates that the superposition principle predicts the downstream coolant efficiencies reasonably well. For multiwindow designs, the superposition principle can, thus, be used as an initial design tool to predict downstream window "external edge" conditions to determine downstream cooling requirements.

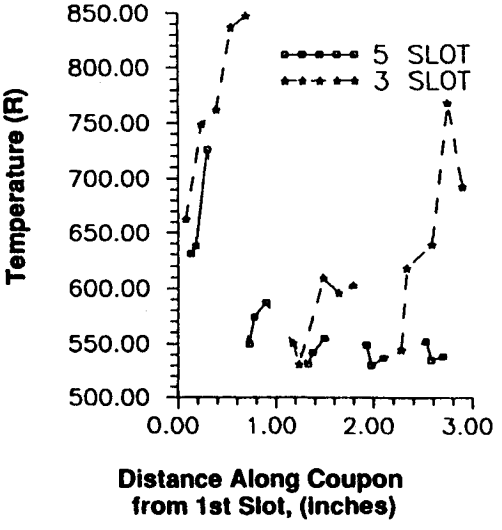

Fig. 14 Multiport ejection temperature data.

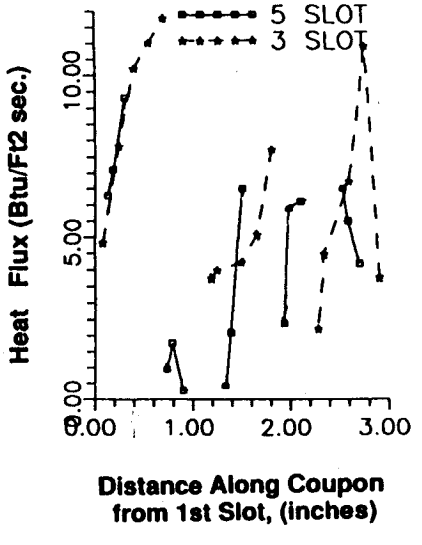

Fig. 15 Multiport ejection heat flux data.

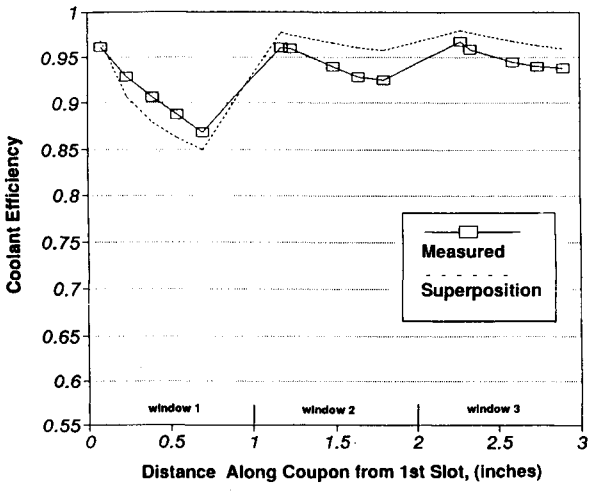

Fig. 16 Superposition principle compared to data.

Using the superposition principle (with measured front slot breakpoints and efficiency slopes), coolant flow rate requirements to cool the designed and tested coupon windows isothermally (to coolant temperatures) for the 4200 Btu/lbm enthalpy arcjet conditions at Ames are as shown in Table 4.

The major result of this test series is the high thermal performance found with NO_2, attributed to its endothermic dissociation. The performance of CO_2 and N_2 can be seen on Table 4 to be similar to each other. Tangential ejection was thermally superior to angled ejection. The superposition principle was shown to be an acceptable initial design tool for multiport ejection whereas 0.6-in. window lengths were thermally more effective than 1.1-in. lengths.

CFD Analysis

Calculations were conducted for the Ames arcjet tests using state-of-the-art CFD procedures. A computer code, KIVA, developed by Los Alamos National Laboratory, has been modified to provide comparisons with the gaseous test data, predictions regarding liquid ejection, and analysis-of-flight configurations.[10]

KIVA solves the equations of transient multicomponent chemically reactive fluid dynamics coupled with the dynamics of an evaporating liquid spray. The code was originally developed for internal combustion engines by the Los Alamos National Laboratory and has been modified by Aerotherm for general applications.[11,12] The formulation is three-dimensional, but both planar and axisymmetric geometries can be considered without unnecessary grid points. KIVA is a time-accurate, finite volume code that uses a partially implicit numerical scheme coupled with an acoustic subcycling procedure for efficient solutions at all Mach numbers. The spatial differences are formed on a general mesh of arbitrary hexahedrons whose vertices are specified as functions of time. This feature allows a Lagrangian, Eulerian, or mixed description and is particularly useful for representing curved or moving boundary surfaces. An arbitrary number of species and chemical reactions are allowed. The reactions may be divided into kinetically controlled or equilibrium reactions, which are treated with different algorithms for numerical efficiency.

Gaseous Coolants

The freestream conditions for the arcjet environment, the arcjet species mole fractions, and the mass flow rates for three different test cases are presented in Tables 5–7, respectively. These conditions were used as boundary conditions on the computational domain. The shock was captured within the prescribed grid. The boundary conditions at the ejection locations were defined by specifying the densities, temperature, and velocity components. The velocities were calculated from the ejected Mach number and the densities were then calculated to match the measured mass flux.

Figures 17–19 present typical contour plots for the arcjet calculations. These specific plots are for an angled injection case with 1.1-in. windows. The coolant was NO_2 which reacts with the boundary-layer gases. Figure 17 presents the temperature contours and shows the bow shock that has formed over the test article. The effect of the coolant is shown in a very thin layer near the wall. Figure 18 shows the corresponding NO_2 mass fractions. The NO_2 is also located in a thin layer near the wall where the temperatures are low. The O_2 mass fractions of Fig. 19 show the dissociation of the oxygen across the shock layer and the recombination near the wall on the front of the test article. Downstream of the injectors, the oxygen is displaced by the NO_2 and a region of low oxygen concentration appears near the wall.

Figures 20–22 compare the predicted heat flux with the measured data. The predicted heat fluxes are in good agreement with the experimental data considering the complexity of the flow especially the expansion of the arc flow from the nozzle. The wall temperatures on the water-cooled leading edge were not measured and the wall temperature boundary conditions over the front of the test article were set to the measured values on the windows. The heat fluxes over the test locations were quite low which indicates the effectiveness of the window cooling. Most of the measurements were less than 15 Btu/ft^2 · s in a 2800 K arcjet flowfield. These low heat flux values mean that scatter in the data or numerical error in the computations would have a more significant effect on the results.

Figure 20 is for a N_2 test with an ejection angle of 30 deg. The calculation shows a large decrease in the heat flux immediately downstream of the ejector which quickly recovers to a plateau on the window. Further downstream, the heat flux begins to increase rather sharply until the next ejector is reached. Just upstream of the ejector is a small separation region that causes an oscillation in the heat flux predictions. The gridding in these locations was not fine enough to resolve these effects and the oscillations are due to parasitic modes in the velocity fields. Arbitrary Lagrangian Eulerian (ALE) codes are very susceptible to this "checkerboarding" effect since they locate the velocities at the vertices of the cell. The calculations predict the same trends over each of the three window

Table 4 Fully cooled flowrate requirements, lbm/s

Coolant	Ejection type	3×1.1-in. windows	5×0.6-in. windows
N_2	Angled	0.42	0.31
N_2	Tangent	0.15	0.11
CO_2	Angled	0.51	0.42
NO_2	Angled	0.06	0.045

Table 5 Arcjet freestream conditions for CFD analysis

Mach no.	3.157
Velocity	3003 m/s
Static pressure	0.0964 atm
Temperature	2641 K

Table 6 Arcjet mole fractions for CFD analysis

N_2	0.7596
O_2	0.1755
N	0.2803E-05
O	0.0375
NO	0.0273

Table 7 Arcjet testing coolant flow rates (lbm/s) for CFD analysis

Window location no.	N_2 angled ejection	NO_2 angled ejection	N_2 tangential ejection	Liquid N_2O_4 ejection
1	0.0490	0.0090	0.0490	0.0170
2	0.0460	0.0083	0.0400	0.0100
3	0.0450	0.0083	0.0400	0.0067

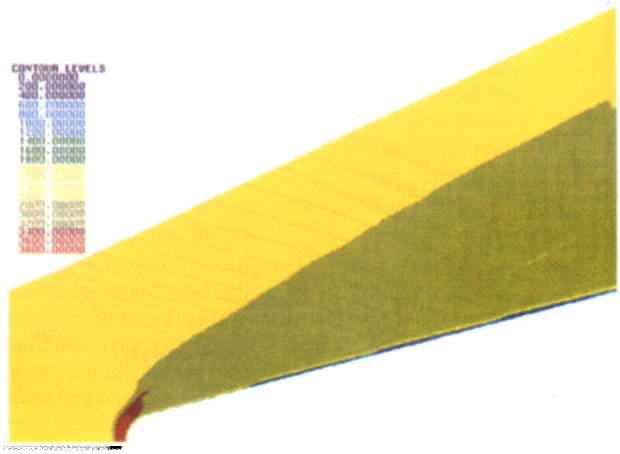

Fig. 17 Temperature contours for NO_2 coolant.

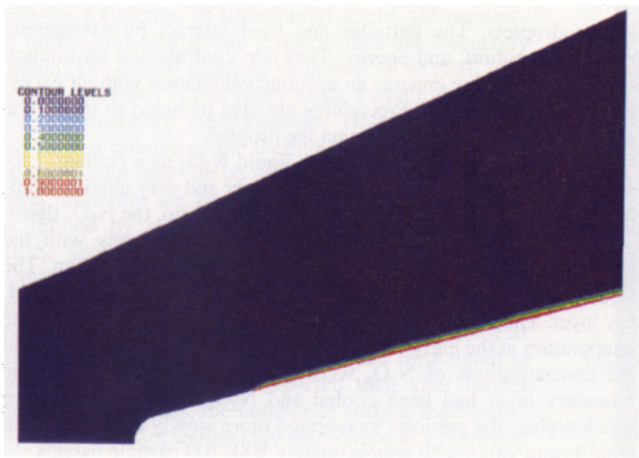

Fig. 18 NO_2 mass fractions for NO_2 coolant.

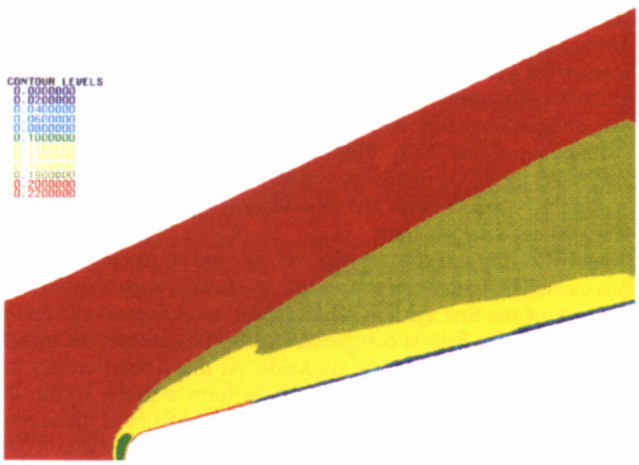

Fig. 19 O_2 mass fractions for NO_2 coolant.

locations. The measured data on the first window has a different behavior than on the other two windows. This may be due to the upstream effects of the leading-edge wall temperatures or the expansion of the arc flowfield. The trends on the aft windows are similar to those predicted by the calculations.

The NO_2 heat flux predictions are compared with the measured values in Fig. 21. For this coolant, there is not a large decrease immediately downstream of the slot as was noted with the N_2 coolant. The predictions are again in better agreement with the measurements at window locations 2 and 3. The first window has

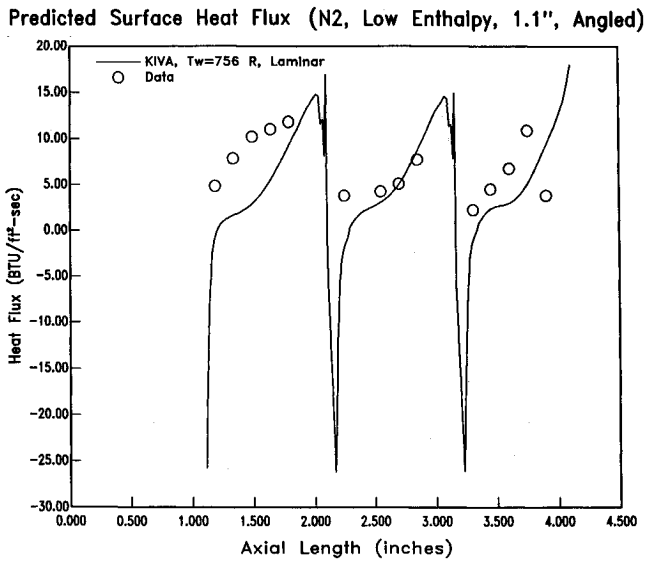

Fig. 20 Comparisons with the experimental data for angled N_2 coolant.

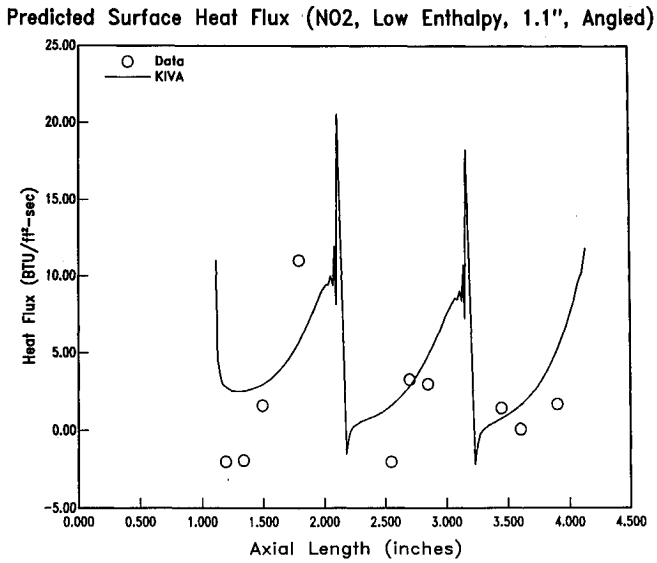

Fig. 21 Comparisons with the experimental data for angled NO_2 coolant.

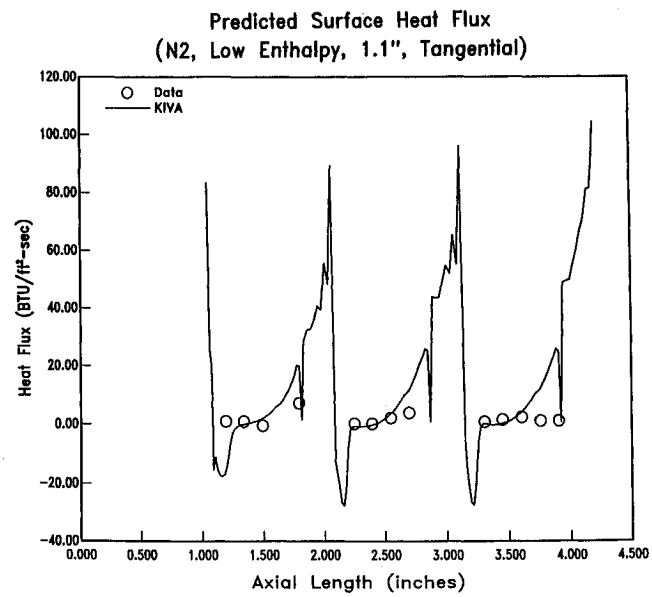

Fig. 22 Comparison with the experimental data for tangential N_2 coolant.

a much steeper increase than was calculated. The heat flux for these conditions had a maximum value of about 10 Btu/ft^2·s, but the mass fluxes were a factor of 5 less than the N_2 case. The NO_2 is shown to be a much more effective coolant than the nonreacting N_2.

The heat flux predictions for N_2 ejected tangential to the coupon surface are shown in Fig. 22. The measured heat fluxes for this case were again low with little variation across the window locations. The predictions are in good agreement over the first half of the windows but show an increase upstream of the slot. The forward facing step (immediately downstream of the last thermocouple) does not perturb the flowfield significantly. The calculations do predict significant heating (50 Btu/ft^2·s) on the raised portion of the model that exists between the windows. No measurements were taken on this part of the model for comparison.

Liquid N_2O_4 Coolant

Evaporating liquid sprays are modeled in KIVA by a discrete-particle technique. Each computational particle represents a number of droplets. The particles and fluid interact by exchanging mass, momentum, and energy. Timestep controls and an implicit coupling procedure ensures an accurate calculation without excessively small timesteps. Procedures are also included to model the effects of flowfield turbulence on the droplets.

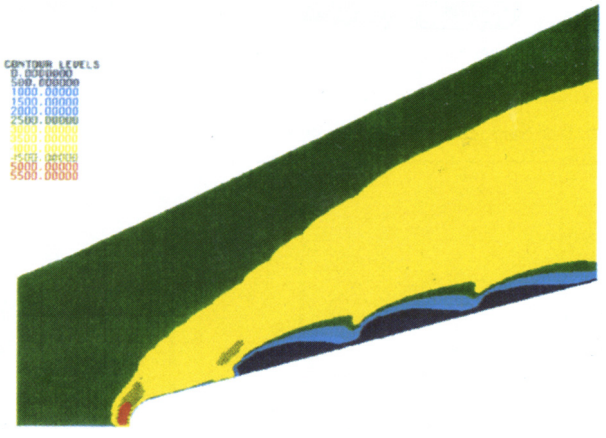

Fig. 23 Temperature contours for liquid N_2O_4 coolant.

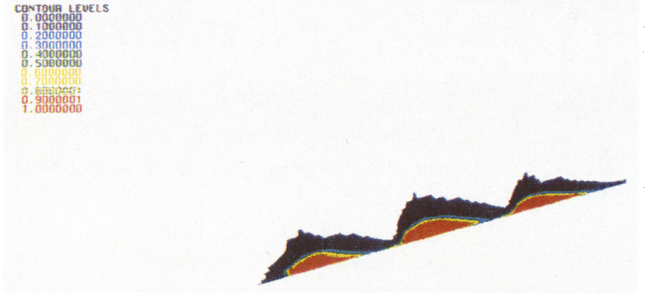

Fig. 24 N_2O_4 mass fractions for liquid N_2O_4 coolant.

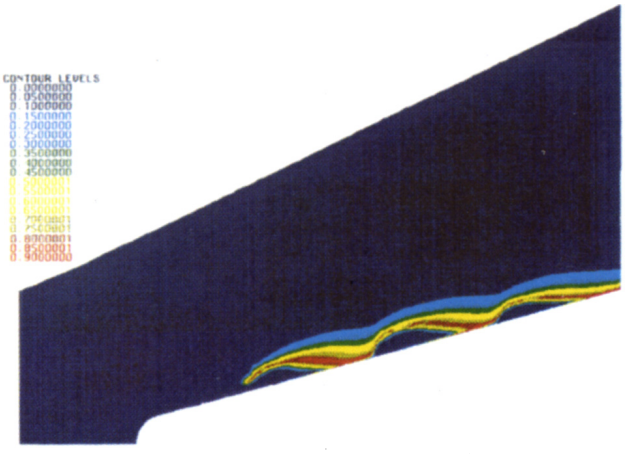

Fig. 25 NO_2 mass fraction for liquid N_2O_4 coolant.

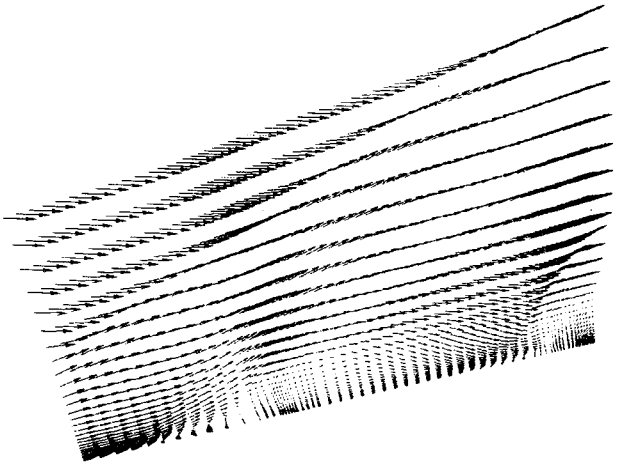

Fig. 26 Velocity vectors over the first window for liquid N_2O_4 coolant.

Calculations have been done for liquid N_2O_4 as a coolant. Liquid N_2O_4 is sprayed into the boundary layer and very quickly evaporates forming gaseous N_2O_4. As the gas heats up, the N_2O_4 dissociates into two molecules of NO_2 which then reacts with the boundary-layer air and dissociates into nitrogen and oxygen. The liquid N_2O_4 was modeled as liquid droplets ejected into the boundary layer. The evaporation model in KIVA predicted an immediate evaporation at the early time when the boundary layer was hot and the concentrations of N_2O_4 were low. At later times, when the boundary layer had been cooled and N_2O_4 concentrations were much higher, the particles evaporated more slowly and reached an equilibrium value with approximately 500–700 particle parcels.

Figures 23–25 present contour plots from this calculation. The evaporation of the N_2O_4 created a region of high pressure near the ejector which diverted the flow and caused a large perturbation over the windows. In Fig. 23, there is an increase in the temperature due to the deflection caused by this high pressure. Figure 24 presents the gaseous N_2O_4 mass fractions. N_2O_4 is formed as the particles evaporate and is located only around the ejectors. The N_2O_4 disappears before the next window location is reached due to its dissociation into NO_2. The NO_2 mass fractions are shown in Fig. 25. As the N_2O_4 dissociates, the NO_2 concentrations increase. As the NO_2 reacts with the boundary layer, its concentration decreases until no NO_2 remains.

Figure 26 presents the velocity vectors and shows the perturbations caused by the evaporating particles. A large separation occurs upstream of the first ejector due to the pressure increase from the evaporation. The flow is compressed as it turns around the bubble and then expands around the backside. At the second ejector the turning of flowfield is strong enough to form a shock within the surrounding flowfield. The separation region in front of the second ejector is much smaller than the one before the first ejector. The predicted adiabatic wall temperature for this case is shown in Fig. 27. The low wall temperatures indicate that the liquid ejectant is an excellent coolant. In fact the predictions indicate that this particular test case was greatly overcooled. The perturbations in the flowfield caused by the large mass fluxes may be significantly reduced while still providing adequate protection for the window. Measured heat fluxes for this case are not presented as reliable data is unavailable.

Flight Analysis

A calculation was done for a sample flight condition. The vehicle consisted of a 0.5-in. nose radius cone with a half angle of 19.2 deg. The 0.5×0.5-in. windows were modeled with a 0.08-in. metal rim separating each window. The ejector ports were 0.03 in.

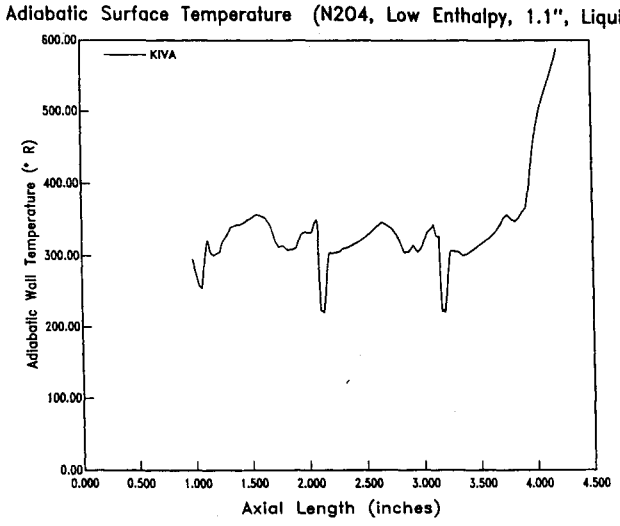

Fig. 27 Predicted adiabatic wall temperatures for liquid N_2O_4 coolant.

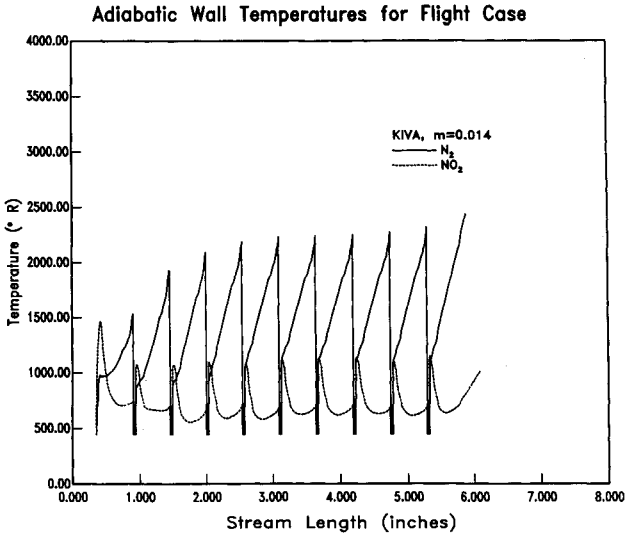

Fig. 28 Adiabatic wall temperatures for a sample flight case with N_2 and NO_2 coolants.

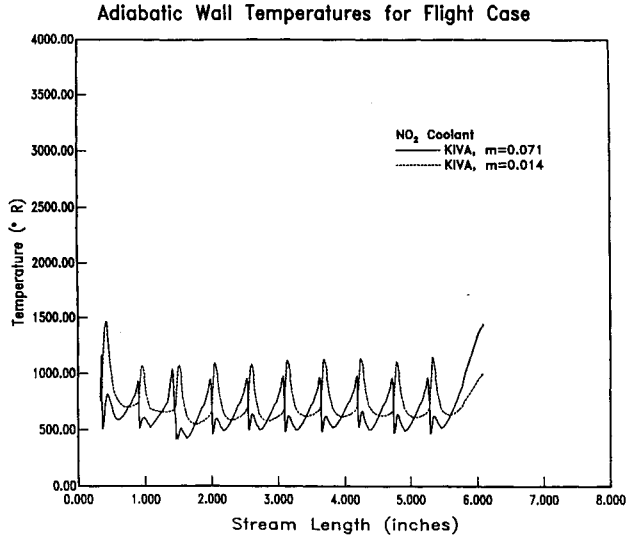

Fig. 29 Adiabatic wall temperatures for a sample flight case with different mass fluxes.

wide and located 0.03 in. from the leading edge of the metal rim. The coolant was ejected at a slot Mach number of 2.0 and at 30 deg to the vehicle surface. Two different coolants were considered, N_2 and NO_2. The mass flowrate for each coolant was 0.014 lbm/s. The conditions used for this sample flight case were 37 kft and 9420 ft/s.

Figure 28 compares the predicted adiabatic wall temperatures from the two cases. The ejector ports can be seen by the low temperatures from the coolant. Immediately downstream of the ejectors, the N_2 and NO_2 cases have similar temperatures. The trends of the two coolants, however, are dramatically different over a majority of the window. The N_2 coolant shows a significant increase in the adiabatic wall temperature over each of the windows, whereas the NO_2 coolant decreases to a value of about 650°R. The wall temperatures begin to increase again just before the next ejector location.

The decrease in the adiabatic wall temperature downstream of the ejector is attributed to the endothermic reaction of the NO_2 with the boundary-layer gases. In the arcjet tests, the NO_2 coolant showed trends similar to the N_2 coolant but was much more effective. For the flight case, the effectiveness of the NO_2 coolant seems to be delayed. This may be due to lower reaction rates at the flight conditions or the higher ejection rates used in the arcjet tests. Increasing the mass flux of the NO_2 reduced the peak somewhat and the wall temperature trends are more like those observed in the arc-heater tests as shown in Fig. 29. This figure also shows that once the windows are sufficiently cooled, increasing the mass flux does not have a significant effect on the wall temperature. A factor of 5 increase in the mass flux lowered the wall temperature only 100°R, even though there is a significant change in the behavior of the flow.

CFD analysis of the NASA Ames thermal test series is in good agreement with the data for both the N_2, an inert coolant, and the NO_2, a chemically reactive coolant. The CFD prediction of the liquid N_2O_4 ejection case suggests a thermal performance even higher than the gaseous NO_2 case.

Future WCT Activity

Future WCT tests will explore the optical performance of the mosaic concept and of reactive coolants. A test series in the 1.5-MW arcjet at Aerotherm will explore IR emission levels of the large NO_2 molecule in the mixing layer of a window cooling system. A flat-plate test series and a full cone test series will be conducted in the AOEC LENS facility to explore aero-optical noise levels. Flight testing may also be added to the WCT program.

Conclusions

WCT tests completed to date have produced much of the data necessary to conduct design trades in the development of the mosaic window cooling system, and, indeed, many of those trades have already been made.

Droplet-sizing tests have established liquid-ejection feasibility and have defined splashplate ejection element geometry. Conservatively ignoring vaporization, droplets ejected from a splashplate element in flight are predicted to be of an acceptable size for IR transmission, based on ground-testing droplet-diameter measurements.

Window pane geometry analysis and optical testing have defined the optical behavior of curved, flat, and polycone window configurations. Based on the blur demonstrated in uncorrected curved windows and on the expected aero-optical and thermal implications of flat windows superimposed on a conical surface, the current baseline configuration of the WCT program is the mosaic polycone.

Thermal arcjet tests have defined ejection geometries and window spacing lengths. The arcjet tests have also identified a reactive coolant, NO_2/N_2O_4, that has outstanding thermal performance and vehicle system packaging advantages. Additionally, tangential ejection has been shown to be superior to angled ejection. The superposition principle has been demonstrated as an effective initial design tool and smaller length windows have been shown to be more thermally effective than longer windows.

CFD analysis has become a vital link between ground-test activity and flight prediction. CFD analysis has replicated the results obtained in thermal arcjet tests not only for inert coolants, but also for the reactive coolant, NO_2. N_2O_4 liquid-ejection analysis has suggested that liquid-ejection N_2O_4 thermal performance is higher than that for gaseous ejection NO_2.

Future IR emission and aero-optical tests will assess the optical characteristics of these reactive coolants and further mature the mosaic window cooling system.

Acknowledgments

The window cooling technology program is funded by, and under the direction of, USASDC, Contract No. DASG60-90-C-0003. The contract monitors have been Troy Street and Greg Jones. The prime contractor is Aerojet Propulsion Division with a program team of McDonnell Douglas Space Systems Company, Aerotherm Corporation, Hughes Aircraft Company, and PRi. The test facilities of NASA Ames, AOEC, Aerotherm, and Aerojet have contributed to this program.

References

[1]Raghuraman, P., Johnson, G. P., and Hodge, R. A., "Coolant Screening Test Report," Aerojet Propulsion Division, KUL:070, Sacramento, CA, Feb. 1992.

[2]Siegel, R., and Howell, J. R., "Scattering from Various Types of Particles," *Thermal Radiation Heat Transfer,* 2nd ed., Hemisphere, Cambridge, MA, 1981, pp. 577–595.

[3]Dodge, L. G., "Representation of Average Drop Sizes in Sprays," AIAA Paper 87-2133, June 1987.

[4]Priem, R. J., and Heidmann, M. F., "Propellant Vaporization as a Design Criterion for Rocket-Engine Combustion Chambers," NASA R-67, 1960.

[5]Sherman, A., and Joseph, S., "Breakup of Liquid Sheets and Jets in a Supersonic Gas Stream," *AIAA Journal,* Vol. 9, No. 4, 1971, pp. 666-673.

[6]Irving, B. R., "A Technical Overview of Code 5, Version 7," *Proceedings of the SPIE,* Vol. 766, 1987, pp. 285–293.

[7]Majeski, J. A., and Weatherford, R. H., "Development of an Empirical Correlation for Film-Cooling Effectiveness," AIAA Paper 88-2624, June 1988.

[8]Murray, A. L., and Saperstein, J. L., "User's Manual for the Updated ABRES Shape Change Code (ASCC 80)," FR-80-38-/AS, Acurex Corp., Mountain View, CA, Oct. 1980.

[9]Sellers, J. P., Jr., "Gaseous Film Cooling with Multiple Injection Stations," *AIAA Journal,* Vol. 1, No. 9, 1963, pp. 2154–2156.

[10]Amsden, A. A., Romshaw, J. D., O'Rourke, P. J., and Dukowicz, J. K., "KIVA: A Computer Program for Two- and Three-Dimensional Fluid Flows with Chemical Reactions and Fuel Sprays," Los Alomos National Lab., LA-10245-MS, Los Alamos, NM, Feb. 1985.

[11]Murray, A. L., and Shannon, R. V., "Generalization of the KIVA Computer Code," 1989 JANNAF Rocket Nozzle Subcommittee Meeting, Naval Surface Warfare Center, Silver Spring, MD, Oct. 1989.

[12]Shannon, R. V., and Murray, A. L., "Development of the KIVA-II CFD Code for Rocket Propulsion Applications," Tenth Workshop for Computational Fluid Dynamics Applications in Rocket Propulsion, Marshall Space Flight Center, Huntsville, AL, April 1992.